GEOPHYSICS, VOL. 84, NO. 3 (MAY-JUNE 2019); P. KS119–KS131, 11 FIGS., 1 TABLE.
10.1190/GEO2018-0517.1

Check for updates

Downloaded 04/04/19 to 171.66.208.130. Redistribution subject to SEG license or copyright; see Terms of Use at http://library.seg.org/

Velocity analysis and subsurface source location improvement using moveout-corrected gathers

Ariel Lellouch[1] and Moshe Reshef[1]

ABSTRACT

The location of subsurface seismic events is important for various geophysical applications. For example, it can be used for underground intrusion detection, monitoring precursors of natural hazards (e.g., sinkholes, rock-falls, landslides, etc.), tracking the structural integrity of mines, locating trapped personnel, and microseismic reservoir monitoring. For a useful analysis, it is imperative that located events be as close as possible to their true spatial position. Although a variety of location methods have been developed, most assume that the correct velocity model is known and are very sensitive to errors in its estimation. Velocity is often estimated at recording borehole locations and calibrated if possible. However, calibration requires manual picking that may induce errors. We use moveout-corrected gathers, whose flatness serves as an objective function, for picking-free velocity model inversion using known source locations. These gathers can be constructed using any implementation of seismic wave propagation. To limit computational costs, we use an eikonal traveltimes solver. The inverse problem is solved using a global optimization approach with an adequate borehole-driven model parameterization. The method performs well in constructing an effective velocity model for location with or without knowledge of the source origin time. We show its application on reservoir-scale synthetic examples as well as a 3D shallow subsurface field one and show the significant final improvement in location accuracy. A single known source is used for calibration of the velocity model. The updated model is not necessarily correct, but it can be effectively used to improve location.

INTRODUCTION

In the mining industry, event location is used to locate trapped miners (Cao et al., 2012) and monitor the structural health of the mine (Šílený and Milev, 2008). Operating in the shallow subsurface, event location may be useful for underground intrusion detection (Tucker et al., 2007) and monitoring precursors for sinkholes (Abelson et al., 2018), rockfalls (Senfaute et al., 2009), and landslides (Tonnellier et al., 2013). Microseismic monitoring is the key technology in imaging hydraulic fractures. Due to the recent industry focus on unconventional resources and the associated need for effective hydraulic fracturing, microseismic monitoring has become a commonplace technology (Maxwell, 2014). Both downhole arrays (Maxwell et al., 2010) and surface receivers (Eisner et al., 2010) have been used to record and subsequently locate microseismic events, each with its own advantages and drawbacks (Eisner et al., 2009a; Diller and Gardner, 2011).

A subsurface event is generated from an unknown source mechanism, at an unknown location (hypocenter), and at an unknown origin time. There are many studies that address the location problem, trying so solve it by different methods. For their majority, they rely on a background velocity model, which is assumed to be known or calibrated (for a thorough overview, see Maxwell, 2014). The standard, most common approach is to use picked arrival times of the P- and S-waves of a microseismic event to estimate the hypocenter location through arrival-time inversion, as is often done in earthquake location (Gibowicz and Kjiko, 1994; Urbancic and Rutledge, 2000). In practice, the often restricted acquisition setup requires extraction of additional information through polarization measurements (Fischer et al., 2008). Using 3C sensors, the wavefront propagation direction of P- and S-phases may be estimated, yielding a directional constraint on the source location. This procedure is mandatory in the common case of single-well monitoring.

Manuscript received by the Editor 12 July 2018; revised manuscript received 2 December 2018; published online 01 April 2019.
[1]Tel Aviv University, Department of Earth Sciences, Tel Aviv, Israel. E-mail: lellouch@gmail.com (corresponding author); moshe@luna.tau.ac.il.
© 2019 Society of Exploration Geophysicists. All rights reserved.

Downloaded 04/04/19 to 171.66.208.130. Redistribution subject to SEG license or copyright; see Terms of Use at http://library.seg.org/

An alternative approach to picking-based location methods is scanning trial sources in space and time and imaging recorded data at those locations (Drew et al., 2005). In its most basic form, given a trial source location and a velocity model, data are aligned along the expected moveout and their amplitude, or energy, is stacked. More elaborate signal coherence measures, such as semblance (Fuller et al., 2007), may also be used. Within a grid of possible source locations and origin times, the point of the maximal stack or coherency response is taken as the hypocenter location. A joint P- and S-wave waveform migration has been suggested (Bardainne et al., 2009), as well as a deconvolution-based migration that uses the joint temporal and spatial origin of both phases (Haldorsen et al., 2013). Finally, more recent studies have tested moment tensor migration imaging, simultaneously inverting for the source mechanism as well as its location and origin time (Chambers et al., 2014; Zhebel and Eisner, 2015). Naturally, in cases of limited acquisition setups, such imaging methods need to be combined with a polarity analysis.

The vast majority of location methods assume the velocity model known. In reservoir monitoring, it is often extracted from sonic logs that require upscaling and blocking (Maxwell, 2014), thus including only depth (1D) variations. In the mining and shallow subsurface section, other well-based techniques, such as vertical seismic profiling (VSP) or reverse VSP, are usually used. Nonetheless, given the subsurface events' distance from the borehole, lateral variations of the velocity model might be significant yet unaccounted for.

In this study, we advocate for complex updates of the initial 1D velocity model, using subsurface sources of known locations, with or without the source origin time knowledge. The calibration process we suggest is, contrary to conventional methods (Hogarth et al., 2017), picking-free. The proposed method operates using moveout-corrected shot gathers, recently introduced for quality control (QC) in microseismic monitoring (Grechka et al., 2015; Shuck et al., 2015). Although these gathers are often used for QC or statics calibration (Jeremic and Duncan, 2017), in this study, we use their flatness, assumed indicative of velocity model correctness, as an objective function. Model updates are then formulated as an inversion problem, aiming at maximizing these gathers' flatness. We solve it using a global-optimization approach, and subsequently use inverted models in conventional location methods.

It is important to note that the suggested inversion approach can operate on picked traveltimes instead of moveout-corrected gathers, as shown for 1D horizontally layered models by Pei et al. (2009). Nonetheless, there are different cases in which traveltime picking is impractical or induces large errors, such as surface microseismic monitoring (Chambers et al., 2010; Shuck et al., 2015), P-wave observation in hydraulic-fracture stimulation (Eisner et al., 2009b), and near-surface event monitoring (Lellouch and Reshef, 2016). In addition, the suggested workflow may be applied using a wave-equation formulation instead of the ray approximation. Although the computational costs are higher, it can handle complex velocity models more accurately.

Several recent studies (e.g., Witten and Shragge, 2017; Lellouch and Landa, 2017; Lellouch and Landa, 2018) aim at using source image properties as a basis for complex velocity model updates. However, the choice of such properties is nontrivial because spatial focusing patterns may vary. In addition, some of them are chosen in extended image domains, which are obtained by applying different imaging conditions. Finally, the source image is constructed by the summation of data recorded at different spatial points after traveltime correction or back-propagation of the recorded data using a wave-equation formulation. Because summed data originate from receivers in various locations, it is possible that velocity errors will affect each trace differently. Because only the summation of all traces can be observed, local velocity errors might remain undetected if they have annulling effects on different traces. As an alternative approach, full-waveform inversion using microseismic events is also being recently developed (Lyu et al., 2018; Wang and Alkhalifah, 2018). Nonetheless, such methods suffer from the coupling between source parameters (location, onset time, source function, focal mechanism, etc.) and propagation medium.

In the following, the suggested workflow is illustrated using synthetic and field examples. The synthetic example is of reservoir scale, whereas the field example is from the shallow subsurface. Because the suggested method is general, it may be applied to different monitoring scenarios with little to no adjustments.

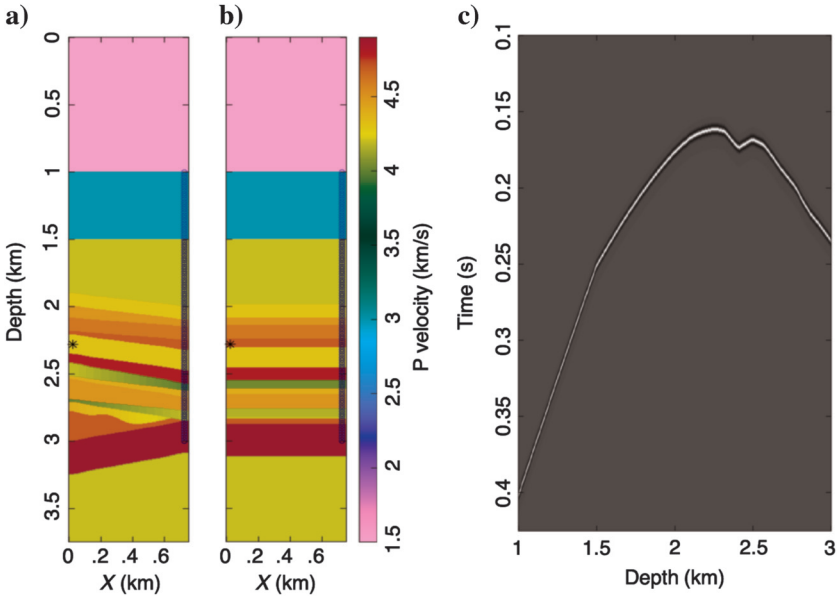

Figure 1. (a) Acquisition setup for single synthetic event recording. The underlying P-wave velocity model exhibits lateral variation due to structural formations. Receiver locations are in blue, whereas sources are denoted by black asterisks. (b) For comparison, an approximated 1D velocity model, extracted at the receiver borehole, is used. (c) Synthetic data are computed using the model in (a).

SOURCE IMAGING AND MOVEOUT-CORRECTED GATHERS

A conventional location method is coherency scanning, also known as source imaging, which is equivalent to a one-way Kirchhoff migration. It estimates the source location at the point of maximal imaged amplitude assuming a known velocity model (Maxwell, 2010). The influence of velocity models on microseismic location has been extensively studied (Eisner et al., 2009a; Poliannikov et al., 2014) and found to significantly affect event positioning. However, reasonable source images might be obtained even when

Downloaded 04/04/19 to 171.66.208.130. Redistribution subject to SEG license or copyright; see Terms of Use at http://library.seg.org/

using wrong velocity models, eventually leading to spatial location errors. Let us demonstrate this with a simple test case. In Figure 1a, we show a wide-coverage, 2D monitoring acquisition of a single event in a relatively complex acoustic velocity model. Receivers are positioned between depths of 1 and 3 km, with a spacing interval of 5 m. We use a 1D approximation of the velocity model (Figure 1b), extracted at the monitoring borehole location, for comparison with the true model. Using the complex velocity model, we generate synthetic data by calculating traveltimes from the designated event location to all monitoring receivers and convolving them with a Ricker wavelet (Figure 1c). Note the complex wavefront arising from the velocity model. Because there is no added noise and a fair number of receivers, the imaging quality practically depends solely on the accuracy of the velocity model.

We construct source images using the coherency scanning method: for every possible source point in space, traveltimes to each receiver are calculated using the velocity model. In this example, we use an eikonal solver. Then, traces are shifted according to calculated traveltimes and are subsequently stacked. In Figure 2, we show the images constructed using the different velocity models. When the image is computed using the true velocity (Figure 2a), the point of maximal stacked amplitude coincides with the true source location (the green cross). However, when the 1D velocity function extracted at the receivers' location is used, the location of the energy maximum, and thus the estimated source location, are mispositioned by approximately 50 m in both axes (Figure 2b). Although in practical cases, the reference true image is unknown, in this example, we see that the stacked energy is lower when the 1D model is used (0.6 versus 1 in normalized values). This indicates a nonoptimal summation of traces at the estimated image point.

By constructing moveout-corrected gathers, one can observe the contribution of each recorded trace to the source image. Practically, those gathers are simple to construct. For every spatial point at which such a gather is to be constructed, we calculate estimated traveltimes from that point to each receiver. Then, each trace in the original shot record is shifted according to the associated traveltime. Let us now revisit the velocity model's effect on source imaging. Looking solely at the image constructed using the wrong velocity model, as would be available in practical cases, there is no direct, simple way of realizing that the model is incorrect. In Figure 2, we also show time-shifted gathers constructed at the estimated source locations (the points of maximal amplitude), using the true (Figure 2c) and 1D velocity models (Figure 2d). When constructed using the former, the gather is flat and centered, after moveout correction, on origin time zero. On the contrary, when the 1D model is used, only a certain part of the gather is flat and some traces are significantly separated, indicating incoherent summation and an erroneous velocity model. In addition, its flat part (receivers 1–250) is centered on approximately 15 ms. Knowledge of the source origin time would have thus also immediately ruled out the gather as centered on a wrong origin time. Without such knowledge, cases of limited acquisition (e.g., using only receivers 1–250) might prove difficult in estimating velocity correctness because the gather may have a practically flat part even when constructed with an erroneous velocity model.

In Figure 3, we show different moveout-corrected gathers constructed using the same single source data to illustrate the gathers' sensitivity. They differ in the location at which they are constructed as well as the used velocity. When the correct velocity model and source location are used, the gather has no residual moveout. On the contrary, when either one of them is wrong, the gathers are bent in some complex way. It is important to note that location errors in

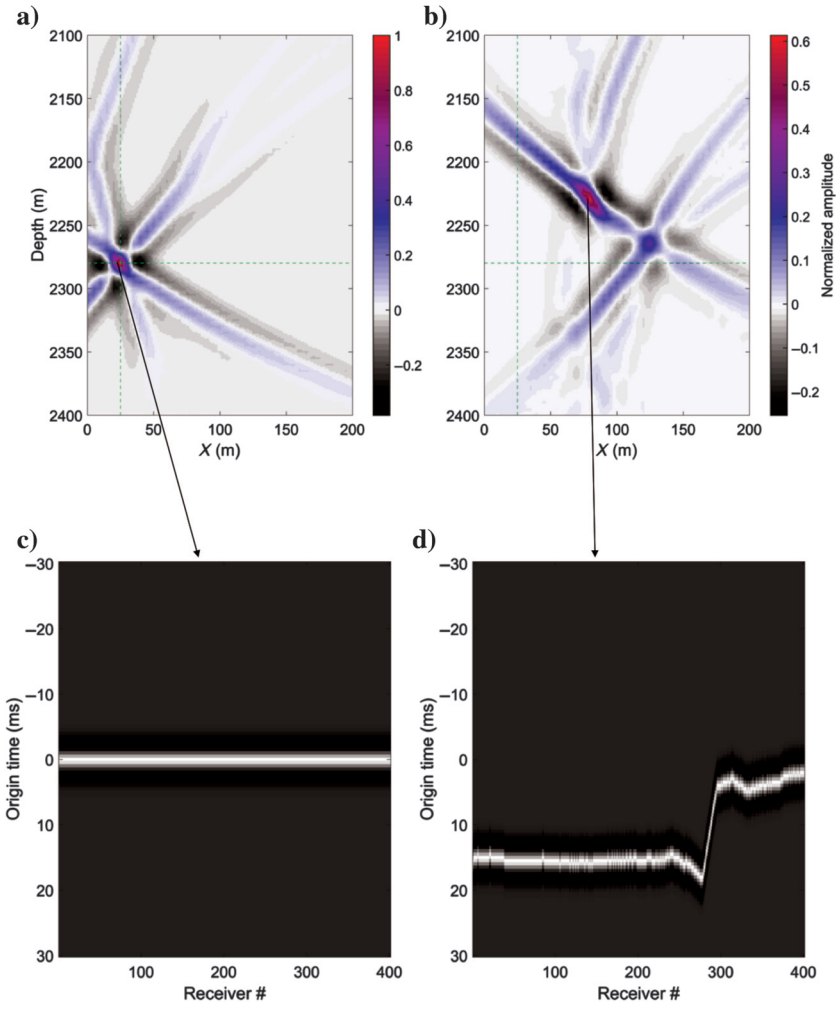

Figure 2. Image contribution decomposition. (a) Imaging of single source data, using the true velocity model. (b) Imaging using a 1D approximation of the velocity model. The true source location is denoted by a green cross. When a 1D model is used, the estimated focusing point is shifted by approximately 50 m in X and Z. The amplitude at the point of maximal focus diminishes, indicating the noncoherent summation of traces. (c and d) Time-shifted gathers constructed at the estimated source locations with true and 1D velocity models. When we use the true model (c), the gather is perfectly flat and at the correct origin time (no moveout). However, when the 1D model is used (d), the gather loses its flat shape. The flat (up to receiver 250) part is focused approximately on 15 ms, which, if origin time is known, also indicates wrong velocity/location.

depth are mapped to much larger moveout changes in the gathers compared with lateral errors. This is indicative of a higher sensitivity to depth estimation, as expected from the acquisition geometry. Negative ("smiling") and positive ("crying") velocity errors have different effects on the gathers' moveout. It is also worth noting that relatively small velocity errors (5%) have a significant influence on the gathers. Nonetheless, for this example, we use a bulk shift of the velocity model, which accentuates the effect on the gathers. In addition, when a wrong model is used, a flatter gather would almost certainly exist at another spatial location, as is the case in the previous example.

In general, because the origin time, velocity model, and source location are coupled in their effects on the gathers, ambiguities may arise. Therefore, introducing correct a priori information by constraining some of the unknowns may be helpful in estimating the remaining ones. For microseismic location, the velocity model is fixed and the location and time are estimated. For velocity model updates, on the other hand, sources of known location may be used. The advantage of knowing their origin time is clear because we know the gathers have to be flat at origin time zero, but it is not necessary. From the simple examples shown so far, we conclude that moveout-corrected gathers are sensitive to velocity errors and can therefore be used as a basis for velocity model updating. However, one should keep in mind the velocity/origin time coupling, and aim at eliminating it, mostly by wider receiver coverage.

In this study, as previously stated, we aim to use moveout-corrected shot gathers directly for velocity model inversion. So far, we have seen that when using the correct velocity model, constructed moveout-corrected gathers are flat. By contrast, causality between flat gathers and correct velocity model has been extensively studied for conventional migration velocity analysis (Brandsberg-Dahl et al., 2003; Symes, 2008). It was found to be dependent upon the model complexity and the choice of the domain (Biondi, 2006) along which the gathers are constructed rather than always true. Because flat common image gathers are often accepted, under certain limitations, as indicative of an effectively correct velocity model, we will follow this approach in this study.

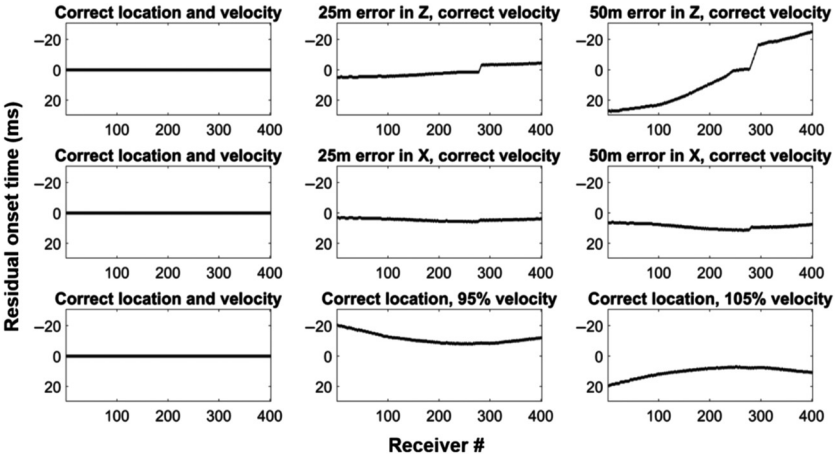

Figure 3. (top row) Gathers constructed at different depths, (middle row) different horizontal positions, and (bottom row) different velocities. Errors in either position or velocity yield nonflat gathers. Gathers are more sensitive to depth errors than horizontal ones, as expected from the acquisition geometry. Negative (smiling) and positive (crying) velocity errors have different effects on the gathers' moveout.

The usage of this type of gathers is different from the standard microseismic velocity calibration approach (Eisner et al., 2009a; Bardainne and Gaucher, 2010). It does not use data traveltimes directly; thus, no picking procedure is conducted. As a by-product, it maintains the original data quality and uncertainty associated with it (finite bandwidth, noise, etc.). In addition, it may help in understanding local velocity model errors, which will be reflected in nonflat parts of the gathers. Nonetheless, it is important to note that, assuming correct traveltime picking, the inversion scheme we subsequently discuss may be reduced to operate on picks rather than moveout-corrected gathers.

VELOCITY MODEL UPDATES

In this section, we formulate the basis for velocity model updates based on the flatness of moveout-corrected gathers. Sources at known locations are used, along with source origin time knowledge, if present. Practically, these may be perforation shots, drill-bits, calibration sources, etc. The workflow is based on competitive particle swarm optimization (CPSO). We follow the practical explanation of the method given by Luu et al. (2016). In short, CPSO is a type of Monte Carlo (or random) iterative search that aims at finding the global extremum of a function that has several local extrema and/or might not be smooth. In our case, we aim at finding the optimal acoustic velocity model in terms of a certain objective function that will be discussed later. For now, we assume that for every velocity model $\bar{V}$, there exists a mapping to the objective function value E. In PSO, several simple entities, referred to as particles, are randomly positioned in the model search space of some function, and each one evaluates the objective function at its current location. Then, each particle determines its movement through the search space by combining its own current and best locations in the search space with the best location of the entire swarm, after applying some random perturbations. The next iteration takes place after all of the particles have been moved. Eventually, the swarm as a whole is likely to move closer to an optimum of the objective function (Poli et al., 2007). The competitive part (CPSO) reinitializes particles that are close to one another (in the search-space sense) if their current estimated objective function values are not among the best in the swarm. There are many other possible metaheuristic approaches, such as genetic algorithms, ant-colony optimization, or neighborhood algorithms (Sen and Stoffa, 2013), which we expect to perform similarly well.

In global optimization methods, a crucial choice is the velocity model parameterization. If we allow for every possible grid point to change, the search will most likely never converge. Therefore, we need to assert some a priori knowledge of the velocity model. Because initial velocity models are often obtained from sonic logging, it is reasonable to assume we have layer tops, as well as a reasonable estimation of their velocity, at the monitoring location. However, these layers may be positively or negatively dipping, and the estimated velocity might be erroneous. Because microseismic monitoring distances are usually relatively short, we assume that the velocity within each layer is constant. Therefore, the

Downloaded 04/04/19 to 171.66.208.130. Redistribution subject to SEG license or copyright; see Terms of Use at http://library.seg.org/

Downloaded 04/04/19 to 171.66.208.130. Redistribution subject to SEG license or copyright; see Terms of Use at http://library.seg.org/

model is parameterized using layer dips and velocities, with the layer tops acting as a constraint. On a side note, recent research in the field of microseismics is concerned with the anisotropic parameters of the velocity models (Wuestefeld et al., 2010; Eisner et al., 2011; Grechka et al., 2011). In this study, we limit ourselves to isotropic velocity updates. Despite that, incorporating an anisotropic parameter search, probably after the best possible isotropic model has been constructed, seems highly promising and easily implementable using the CPSO approach.

The remaining issue to address is the objective function. As previously discussed, the gather is assumed to have no moveout when the imaging point and velocity are correct. Therefore, a way to quantify its flatness is required. In search for a picking-free method, we opted for the minimal variation objective function. Let us examine a moveout-corrected gather $d_{i,t}$, with i being the receiver number (out of N) and t being the time-sample number. We assume the gather is calculated within a large time window $[-T, T]$, around an arbitrary but reasonable origin time point. Usually, T would be half a second or so. Of course, if the origin time or a rough estimate of the origin time is available, T can be diminished to reduce computation time. To ensure that the variation objective function is calculated for a significant part of the gather, we first calculate the average trace a_t by

$$a_t = \frac{\sum_{m=1}^{N} d_{m,t}}{N}. \tag{1}$$

We calculate the variation around time s, which is the time sample at which a_t is maximal. To include mostly signal and avoid noise contamination, a rather small window $[s - W, s + W]$ is used to calculate the variation. In this study, we take W as the seismic wavelet length, so that the total window is about twice that wavelet, or approximately 40 ms. The objective function E is then calculated according to

$$E = \sqrt{\frac{\sum_{i=1}^{N} \sum_{t=s-W}^{s+W} (d_{i,t} - a_t)^2}{N \cdot (2W + 1)}}. \tag{2}$$

This is, in fact, the average windowed difference, in the root-mean-square sense, between each trace in the moveout-corrected gather and the average trace calculated by summation of all traces along the receiver axis. Because the same source is recorded by all receivers, we expect it to have the same temporal behavior in all traces. To eliminate amplitude variations due to geometric spreading, varying receiver coupling, anelastic dissipation etc., we normalize each trace before calculating E, which we are minimizing.

With the definition of the objective function E, CPSO may be applied. To illustrate the workflow, we use a source of known location (see Figure 4a), with and without knowledge of the true source origin time. The velocity model is in the background and is fully recoverable using the chosen model parameterization discussed in the next paragraph. We use a set of 100 microseismic events, originating from the same layer, which will eventually be located (Figure 4b). In Figure 4c, we display the initial model, a 1D velocity profile extracted with errors and without dip information at the receivers' location. Recent advances in microseismic monitoring using distributed acoustic sensing (DAS) demonstrate a large increase in receiver coverage. For example, Karrenbach et al. (2017) show a high signal-to-noise ratio recording of a microseismic event over several kilometers covered by an optical fiber. Nonetheless, we choose a wide acquisition geometry mostly for illustrative purposes.

We emphasize that for generating seismograms of recorded events, we use a simple eikonal traveltime solver, whose result is convolved with a Ricker wavelet to yield synthetic data. Therefore, although we introduce P- and S-wave solutions, this is not a wave-equation modeling. Furthermore, inversion is conducted using the same eikonal solver, thus leading to an inverse crime. The reason for this choice is to separate effects of ray approximation and possible cycle skipping from the traveltime resolution of the inverse formulation. We later show the application of the method on elastic modeling data and discuss its limitations.

In Table 1, we summarize inversion parameters, with a total of approximately 30 inverted unknowns. The true model parameters are given, and layer tops are assumed known for the inversion. An initial velocity model, including no dip knowledge and erroneous velocity values, is used as a basis for the CPSO algorithm. Each particle uses a random variation of the initial model as a starting model. The acceptable dip range is $\pm 20^{o}$, and the initial velocities may differ by up to 30% of the initial model values. From this point onward, those constraints are the initial model's only effect on the inversion scheme. For approximately 30 unknowns, we use 300 particles and 500 iterations; i.e., 150,000 different models are tested. This consumes roughly an hour on a standard six-core workstation.

In Figure 5, we show the original calibration shot record and moveout-corrected gathers constructed using different velocities. Input calibration data (Figure 5a) are contaminated with a normally distributed noise. The average signal-to-noise ratio, calculated by

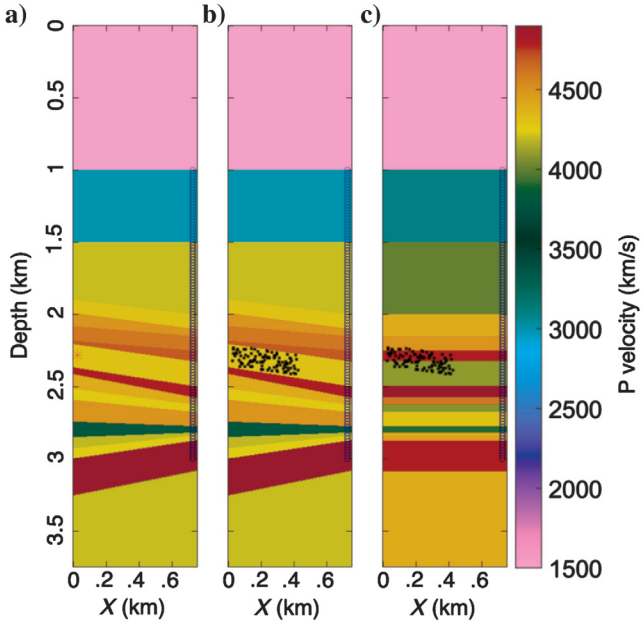

Figure 4. Synthetic test layout. Receivers are denoted in blue circles. (a) Perforation shot (red star) at a known location. The underlying velocity field consists of layers with different dips. (b) Using that model, we simulate 100 microseismic events (black stars), which all originate from the same layer. (c) At the receivers' location, we extract an 1D approximation of the velocity field, containing true layer tops, some velocity errors, and no dip information.

the peak signal value divided by the mean noise value, is approximately 1/2. The first arrivals are hardly noticeable. Automatic traveltime picking of such data is challenging. We applied several methods, which all failed: entropy maximization, the modified Coppens algorithm (Sabbione and Velis, 2010), and short time average over long time average (Earle and Shearer, 1994). The only approach that yields reasonable results for these data is dynamic linear programming, which optimizes the coherency between adjacent traces. We follow Molyneux and Schmitt (1999), but we use a linear objective function based on the total signal amplitude instead. We

Table 1. Summary of layered model properties (the tops are assumed known; although the approximate layer velocities are available, no dip information is present).

Layer #	Top depth (m)	True velocity (m/s)	True dip (°)	Initial velocity (±30%)	Initial dip (±20)
1	1000.0	3000.0	0.0	3100.0	0.0
2	1500.0	4200.0	0.0	4000.0	0.0
3	2000.0	4300.0	8.13	4400.0	0.0
4	2100.0	4500.0	8.53	4400.0	0.0
5	2150.0	4600.0	5.30	4500.0	0.0
6	2250.0	4700.0	5.30	4800.0	0.0
7	2325.0	4300.0	9.32	4100.0	0.0
8	2495.0	4800.0	10.12	5000.0	0.0
9	2575.0	4403.0	12.48	4600.0	0.0
10	2625.0	4272.0	8.53	4050.0	0.0
11	2675.0	4500.0	6.51	4300.0	0.0
12	2775.0	3807.0	2.45	3900.0	0.0
13	2820.0	4187.0	−2.45	4400.0	0.0
14	2840.0	4246.0	−6.92	4450.0	0.0
15	2875.0	4900.0	−9.72	4800.0	0.0
16	3090.0	4200.0	−12.875	4400.0	0.0

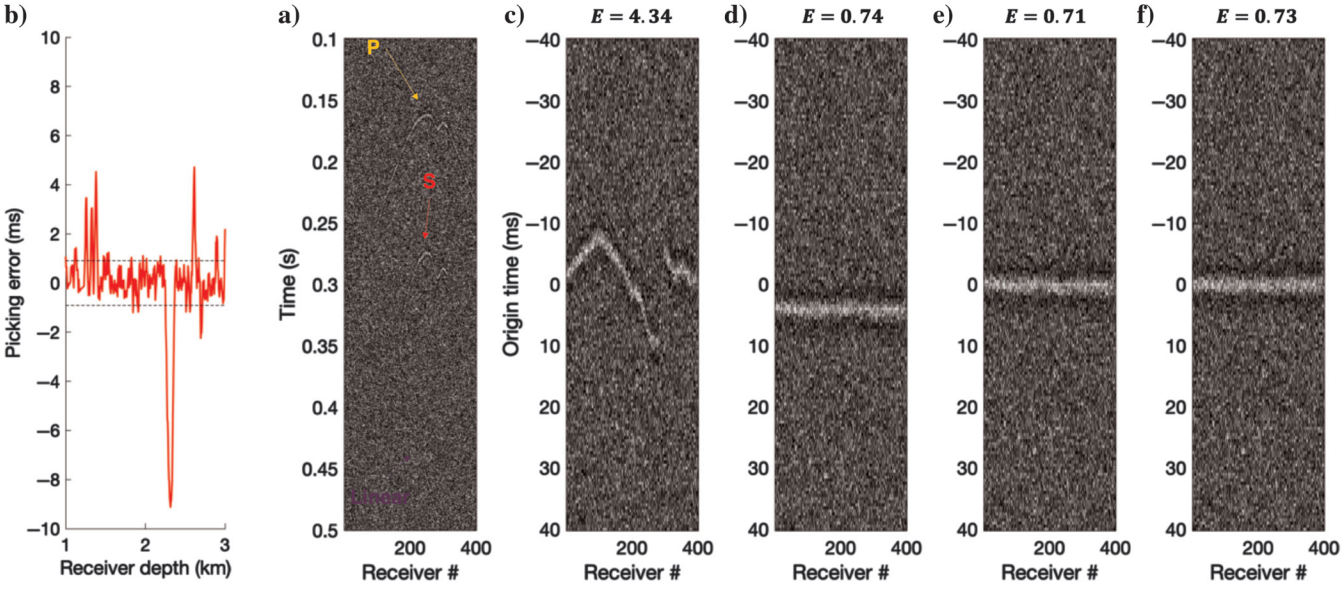

Figure 5. (a) Original shot record of the calibration source. It contains P and S arrivals, as well as a linear moveout noise, all marked by arrows. Signal to noise is very low. (b) Applying autopicking on this record yields large errors. Dotted black lines represent the mean absolute picking error value, which is approximately 1 ms. (c) Moveout-corrected gather, calculated with the initial (1D) model, is clearly flawed because the traces are not aligned. (d) After velocity calibration without source origin time, the gather has a much flatter moveout. However, it is centered approximately 3 ms later than the true origin time. (e) Gather built after origin time information is used to constrain the inversion. (f) Gather built using the true model. Objective function values E, calculated for each moveout-corrected gather, are displayed on top of gathers (c-f).

Downloaded 04/04/19 to 171.66.208.130. Redistribution subject to SEG license or copyright; see Terms of Use at http://library.seg.org/

Downloaded 04/04/19 to 171.66.208.130. Redistribution subject to SEG license or copyright; see Terms of Use at http://library.seg.org/

show picking misfits using this approach in Figure 5b. Figure 5c displays a moveout-corrected gather constructed using the initial velocity model. Traces are clearly misaligned and the gather is very far from flat, indicating a velocity error. After the inversion process, without (Figure 5d) and with (Figure 5e) source origin time knowledge, the gathers are significantly flatter and practically equivalent in quality to the one constructed using the true velocity model (Figure 5f). This can be seen by the objective values obtained for each gather, which are very close for these three models. However, when no source origin time constraint is applied, the gather (Figure 5c) is centered on the wrong origin time, with a misfit of approximately 3 ms, indicative of a too-high velocity model. It is also important to note that the S and linear phases, despite being present in the data and not being manually overridden, are never coherent after moveout correction with the P-wave velocity, and thus they do not affect convergence. The averaging nature of the chosen objective function allows for handling of low signal-to-noise ratio data because when enough receivers are present, the noise effects are canceled out.

Let us now examine the velocity models whose usage yields these gathers. In Figure 6a, we show the initial, 1D, erroneous model. Inverted models, with (Figure 6b) and without (Figure 6c) source origin time knowledge, are quite different from the true model (Figure 6d) despite capturing the overall model trend. Although some of the discrepancies may be attributed to global optimization convergence, which is random and eventually limited by the run time, the gathers may shed some light on the uniqueness of the inversion. In terms of the objective function, gathers constructed using the inverted models are practically as good as the one constructed using the true model. Due to noisy input data, a better objective function value is actually obtained for one of the inverted gathers. In other words, nonuniqueness is an inherent part of the inversion problem as formulated. It is also reasonable to assume that many different models might yield practically equivalent objective function values. As a result, correctly retrieving the model becomes an impossible task.

Therefore, we refer to the inverted velocity model as an effective one, applicable for location purposes, and not a true structural/depth model. Because we are eventually interested in improving the location, it is acceptable to use objectively wrong velocity models as long as they are effectively useful for location purposes within a given area. In addition, due to the objective function's complexity, it is possible that the inverted solution is only a local minimum and equal or better (in terms of minimum variation) models exist. Nonetheless, because we use a global-optimization solution, it is less likely.

LOCATION IMPROVEMENT

We use inverted velocity models for coherency scanning-, or source imaging-based location of all 100 modeled microseismic events (Figure 4b), using no origin time knowledge of the sources. Located events have the same signal-to-noise ratio and contain different seismic phases, as does the calibration source. By the nature of the location method, picking is not applied and the procedure is, for this example, fully automatic. In Figure 7, we show a summary of location results. Using the initial velocity model (Figure 7a), location is very poor and the average error, measured as the 2D distance between true and estimated locations, is approximately 100 m. When the inverted velocity models are used, the error decreases dramatically — to 20 m without the source origin time (Figure 7b) and 13 m with it (Figure 7c). Due to noisy input data, even when we use the true model (Figure 7d), the location is imperfect and has an average error of 11 m. In Figure 7e–7h, we show histograms of error distribution in the x- and z-directions. In addition to the obvious improvement when using the calibrated models, we also see that location is more precise in its depth estimation than its lateral one. Because the acquisition system has superior resolution in the z-direction, this result is expected (Eisner et al., 2009a). Overall, we conclude that even though the calibrated velocity models differ from the true model, they clearly improve the location results and may thus be used for that purpose. Although error distribution after calibration is not significant enough for a thorough statistical analysis, we expect a decrease in accuracy the further the sources to locate are from the calibration source's location.

ELASTIC EFFECTS

As previously stated, the synthetic example that we show is guilty of the inverse crime. Therefore, we repeat the calibration procedure with simulated data computed using a wave-equation 2D pseudospectral elastic modeling. The source is a force wavelet directed toward the receiver borehole. In Figure 8a, we show the modeled recorded data. By superimposing eikonal traveltimes on it, we show that the ray approximation cannot accurately retrieve wave propagation in complex areas. To use elastic data for velocity calibration, we take its absolute value and normalize each trace by its maximum to avoid angle-dependent phase and amplitude effects. When these data are used with the same initial velocity model as the previous example (Figure 8b), the gather clearly is not flat. After calibration without source origin time (Figure 8c), the gather is flatter, but the problematic area remains unresolved. Even when using the true model (Figure 8d), the gather is not flat and it has a significantly worse objective function value compared with the inverted model.

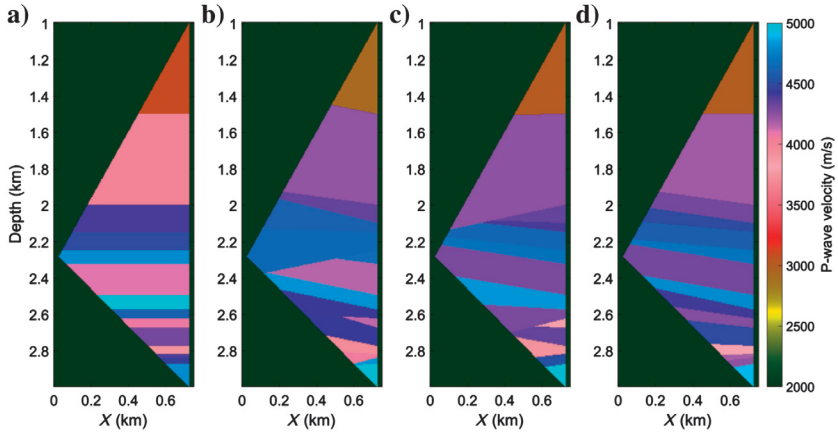

Figure 6. Original and inverted velocity models. We only display the approximate illuminated parts of the model using a single calibration source. (a) Initial erroneous 1D model. (b) Inverted model using the calibration source, without the source origin time information. (c) Inverted model using source time information as well. (d) True model. The overall velocity trend and dips are relatively well-resolved, especially with the source origin time knowledge.

Downloaded 04/04/19 to 171.66.208.130. Redistribution subject to SEG license or copyright; see Terms of Use at http://library.seg.org/

This is due to the limitations of the ray approximation that we use during the inversion procedure.

For a fair comparison, located events are unchanged and remain computed using a ray approximation. Nonetheless, event location using a calibrated model obtained with an elastic calibration shot is significantly improved. Although for the initial model, the average error is approximately 100 m, Figure 8e shows a decrease to approximately 30 m using the calibrated model and its error-distribution histogram (Figure 8f). This is not much worse than the average 20 m error obtained, in the previous section, with a calibration source of unknown time computed using the forward modeling of the inverse operator.

3D FIELD-DATA EXAMPLE

The field example we show is in the shallow subsurface. The study is conducted around a 10 m diameter shaft used for construction, with manual hammer hits used as the sources. The hits, whose locations are known, are oriented toward the receivers, positioned in three separate cased boreholes (Figure 9a), named BH 1 to BH 3. A 16 3C geophone string is positioned at a different depth in each borehole (Figure 9b) and coupled to its casing using pressurized air. The lithology of the area is a mixture of sand, shales, and occasionally sandstones, without clear boundaries between units. Due to overburden pressure and compaction, the velocity increases with depth. At the surface level, we observe very low velocities, representative of unconsolidated sediments (Lellouch and Reshef, 2017).

The synthetic example shown above is of a 2D scenario. However, the transition to 3D is relatively straightforward. As data preprocessing removes amplitude information, the problem becomes essentially kinematic. Thus, as long as traveltimes can be calculated for a 3D model, there is no major difference between 2D and 3D applications.

Due to the 3D nature of the problem and data scarcity, we operate in a two-stage approach. At first, we invert for an optimal 1D velocity model using all available data because most subsurface complexity lies in the depth variation. The model consists of 51 layers, each 1 m thick, spanning depths of 0 −50 m. To obtain geologically realistic models, a 10 m smoothing window is applied to the velocity field. The initial model for the first stage of the inversion is a 1D average of several check shots conducted in the area. For each layer, the inverted velocity is constrained to ±30% of the initial velocity model at that layer. After the best 1D model is established by inversion, we repeat the procedure for each borehole separately. Therefore, for each azimuth, a different 1D model is constructed. The best overall 1D model, previously estimated during the first stage, will be used as a ±10% constraint for the azimuthally dependent second-stage inversion. In addition, the estimated source origin time (i.e., the time at which the gathers are flat) from the first stage is used as an constraint for each azimuth separately. Under these conditions, we allow for relatively small variations of the best 1D model and assure separately inverted gathers are focused on the same origin time. The three separate 1D models, one per azimuth, are combined using a kriging procedure, assuming each extracted profile originates at the midpoint between the source and receiver boreholes.

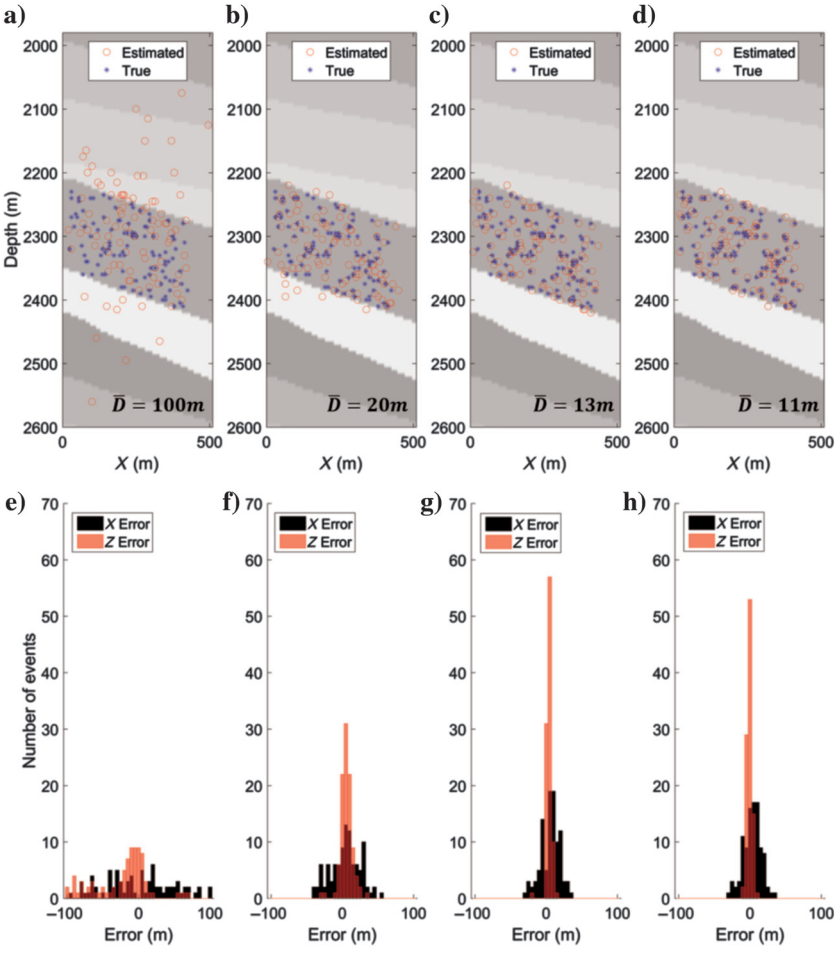

Figure 7. Final location results for different velocity models: (a) initial (1D) model, (b) inverted model without origin time, (c) inverted model with the origin time, and (d) true model. Correct source locations are denoted by blue stars, and estimated locations are denoted by red circles. The average location error (2D distance) is denoted by D on top of each graph. Below each location plot, a histogram of positioning errors in X (black) and Z (red) is drawn (e-h). Overall, errors using the initial model are very large and follow a relatively flat distribution. When calibrated models are used, errors decrease significantly and the distributions are more Gaussian-shaped.

Figure 10 summarizes the calibration process using a single shot at a depth of 9 m with unknown origin time as the calibration information. In this example, we study only the *Z*-component data of the first-break (P-wave) arrival because it is illustrative of the presented concepts. In addition, as can be seen in the calibration source record (Figure 10a), the data quality for the S-waves picking is lower and it is debatable whether the arrivals have any moveout at all. Due to the lack of separation between the first arrival and later phases, dead/noisy traces, and polarity reversal, recorded data cannot be used directly. Although traveltime picking is not conducted,

Downloaded 04/04/19 to 171.66.208.130. Redistribution subject to SEG license or copyright; see Terms of Use at http://library.seg.org/

preprocessing is required and the workflow is not, in this case, automatic. We show the same data, after choosing high-quality traces (39 out of 48 are used), manually applying top and bottom mute, and correcting the traces' polarity for sign reversal, in Figure 10b. The moveout-corrected gather constructed using the initial velocity model (Figure 10c) indicates that the initial velocity model is erroneous because borehole 3 is clearly misaligned with boreholes 1 and 2. The gather after overall 1D model calibration (Figure 10d) is much flatter. In addition, it is centered on an earlier time, indicating an average velocity decrease trend. When the 3D model is used (Figure 10e), small misalignments are eliminated and the gather flatness is improved. The initial and different inverted velocity models appear in Figure 10f. Analyzing the 1D inverted model, we see that the velocity at depths of 10–30 m is significantly reduced, and deeper values are consistent with the initial model. When 3D variations are introduced, small discrepancies between different azimuths are present. Despite major updates, inverted velocity models are not necessarily closer to reality than the initial model. Nonetheless, following the synthetic examples, they are expected to outperform the initial model in terms of the final location accuracy.

The coherency-scanning location procedure uses data after the same preprocessing applied to the calibration source. Data thus consist of acceptable signal-to-noise ratio traces, muted around the first arrivals, and phase corrected. As such, they may be effectively stacked. We display the location results in Figure 11, with map (Figure 11a) and side (Figure 11b) views. They indicate that for this data

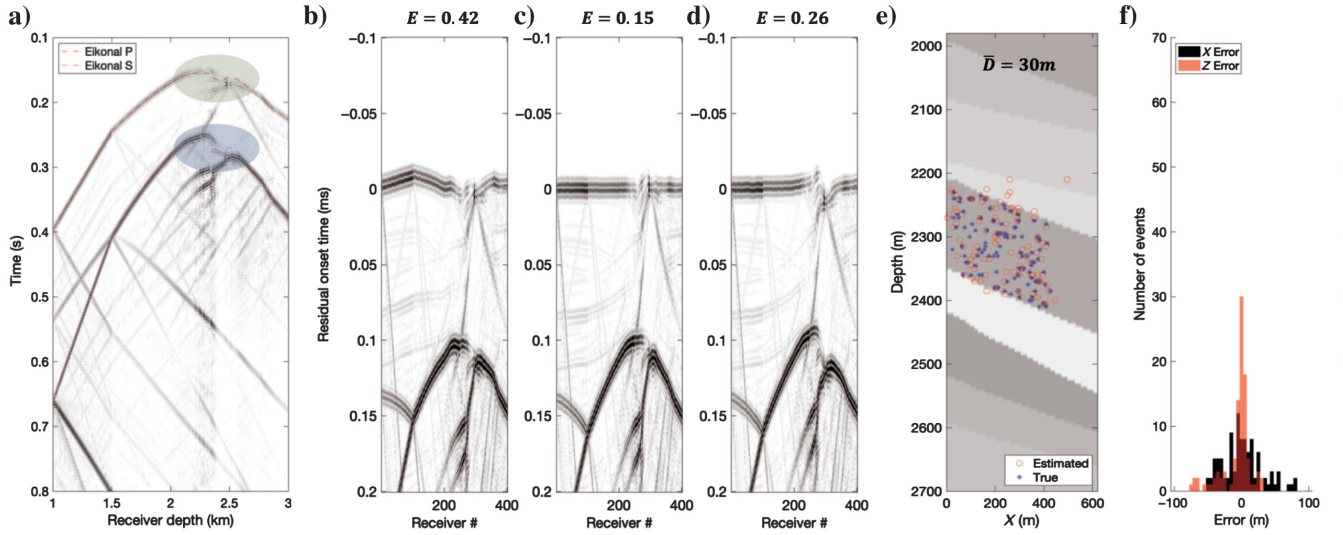

Figure 8. Velocity calibration and event location using elastic calibration data. (a) Modeled data with an overlay of traveltimes computed used an eikonal solver (dotted lines). In the marked areas, the ray-approximation solution significantly diverges from the wave-equation one. (b-d) Moveout corrected gathers built using the (b) initial, (c) inverted, and (d) true velocity models. Objective function values are given on top of the gathers. The inverted velocity model yields higher coherence than the true one. (e) Event location result when using the inverted model. True source locations are denoted in blue stars and their estimated locations in red circles. Average location error is 30 m. (f) Histogram distribution of location errors.

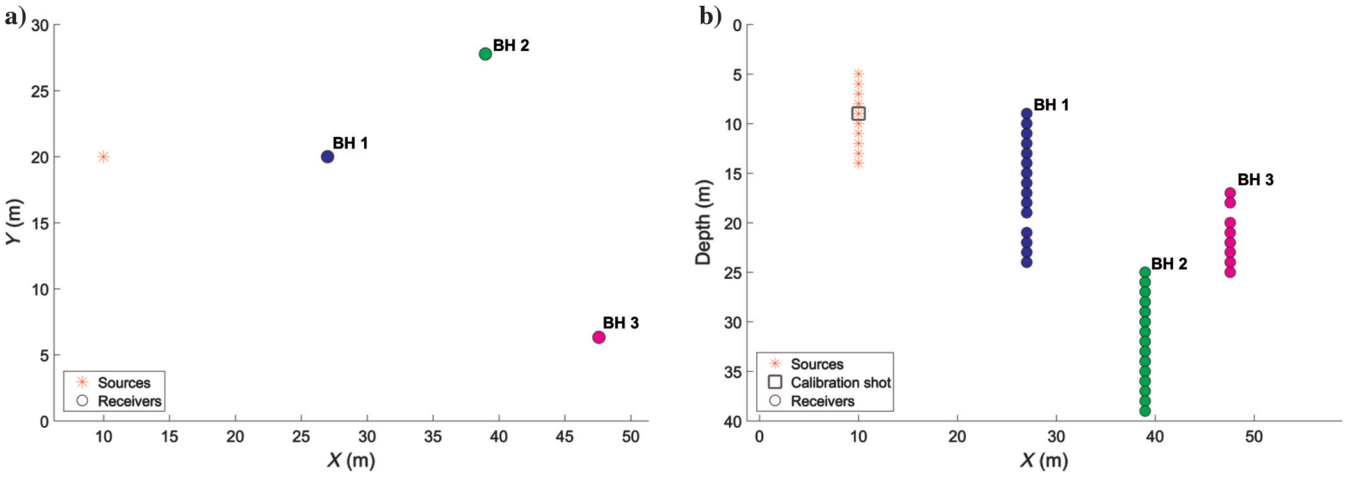

Figure 9. Field-acquisition geometry. Three separate boreholes, denoted by colored circles, record sources at depths 5–14 m, denoted by red asterisks. (a) Map and (b) side view show the experiment layout, including the shot chosen for calibration (black rectangle). Note the overall small scale of the problem, differing from the synthetic example.

Downloaded 04/04/19 to 171.66.208.130. Redistribution subject to SEG license or copyright; see Terms of Use at http://library.seg.org/

set, the initial velocity model is useless in terms of location. Events are mostly positioned very close to the surface and at a wrong $\{X, Y\}$ location. We believe that this is mostly due to the farthest borehole (3), which is, before calibration, significantly misaligned with the two other boreholes. Therefore, intuitively, source locations are drawn toward borehole 3 to compensate for this misalignment. On the contrary, when the calibrated 1D velocity model is used, positioning significantly improves, except for two shallow events. For the 3D model, those events are clustered with the rest and an overall acceptable location is obtained. The mean error, measured as the 3D distance between the true and estimated source locations, is 3.4 m. It is important to note that because of the acquisition geometry, no ray coverage exists below the calibration source depth. Therefore, sources at depths of 2–9 m are inherently harder to precisely locate because the velocity model at these depths cannot be reliably inverted (and thus we use the problematic initial model instead). Accordingly, for 1D and 3D inverted models, the shallow sources are located with a larger error than the deep ones.

Because the difference in location between initial and inverted models is substantial, we conclude that for such scenarios a calibration source of known location is necessary. It is important to note that due to the operational limits of the experiment, the used calibration source is ideal as it is one of the location targets. In cases where the calibration source and location targets are spatially

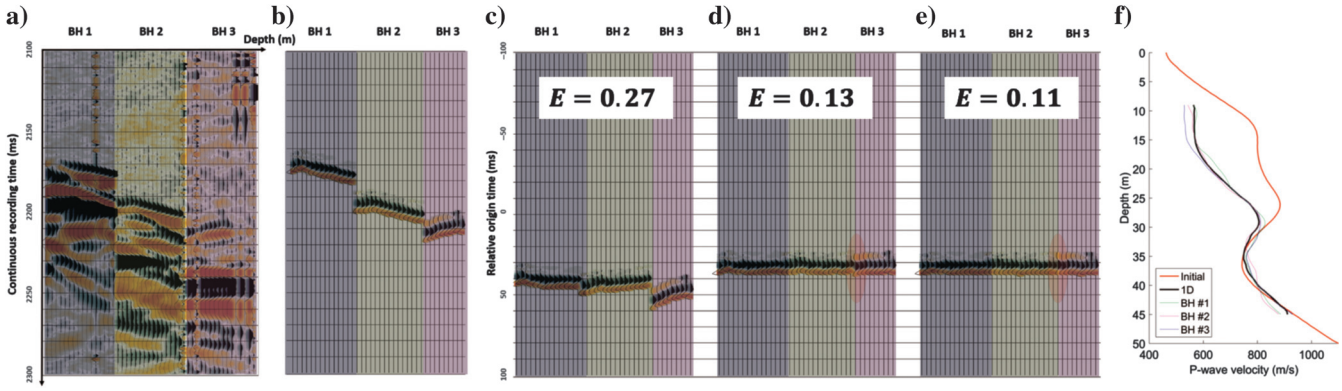

Figure 10. Velocity model calibration. (a) Original shot record. (b) Same record after choosing high-quality traces, muting around the first breaks and manually correcting polarity shifts. (c) Moveout corrected gather constructed using the initial velocity model has significant moveout. (d) Gather after a 1D model calibration without source origin time. It is significantly flatter and centered on an earlier origin time, indicating an overall velocity decrease. (e) Gather after 3D model calibration. Small misalignments in the gather are corrected (see the red ellipses) and flatness is improved. The value of the objective function E is displayed on top of the gathers. (f) Velocity models: initial (red), 1D inverted (black), and azimuthally dependent 1D velocity models (green, magenta, and blue).

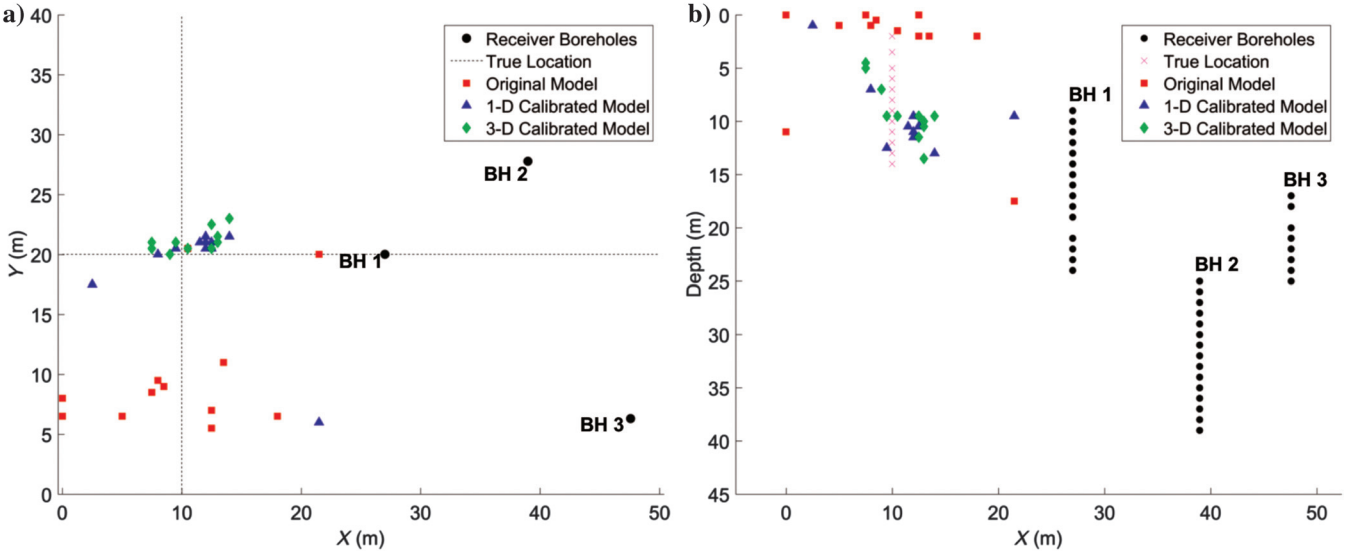

Figure 11. Location results of all 12 events in (a) map and (b) side views. True locations are denoted by the (a) cross' intersection and (b) magenta crosses. Using the initial model, almost all events (red squares) are positioned close to the surface and at a wrong $\{X, Y\}$ location. Using the 1D inverted model, location results (blue triangles) improve significantly. Nonetheless, two events are still mispositioned. When the 3D model is used (green diamonds), those two events are clustered with the rest. The overall location is acceptable — the mean error, measured as 3D Euclidean distance between the estimated and known locations of the subsurface sources, is approximately 3.4 m.

Downloaded 04/04/19 to 171.66.208.130. Redistribution subject to SEG license or copyright; see Terms of Use at http://library.seg.org/

separated, the benefits obtained from such calibration might be diminished. In addition, incorporating the 3D model complexity improves the location results and is recommended whenever possible.

We believe that this example is especially challenging due to the lack of temporal separation between seismic phases. For reservoir- or mine-scale monitoring, on the contrary, a clearer phase separation can be expected thanks to longer propagation traveltimes. Therefore, we expect muting will not be necessary in such cases, whereas some manual trace editing might still be required.

DISCUSSION

So far, we have illustrated how velocity model updates using a single calibration source, with or without source origin time knowledge, can significantly improve the event location. Our examples, synthetic and field, are of downhole monitoring. The method does not require traveltime picking, which is time consuming and is often a source of uncertainty and error. In addition, the used objective function operates simultaneously on the entire moveout-corrected gather. It measures the gather's variation from a pilot trace that is obtained by stacking the gather. As with every summation operator, it allows for better handling of low signal-to-noise-ratio data, often present in monitoring configurations. Conventional picking-based procedures, on the contrary, require single-trace analysis. In the case of low signal-to-noise-ratio shot records, such picking might prove difficult, and thus it might induce errors. A final benefit is that moveout-corrected gathers may be visually inspected for QC. Because they maintain the original data and not its reduction to the traveltime, flatness may be evaluated taking into account the seismic wavelet and data quality. Problematic parts of the gather may be identified, and they may be at least coarsely related to erroneous zones in the velocity model.

Moveout-corrected gathers are versatile in handling varying levels of source information. Because the origin time is a parameter of the gather, the method may be used with and without source origin time knowledge. If it is known, the gather must be flat at time zero after moveout correction. Without knowing the origin time, the gather must be flat at a certain but unknown time. If sources excited at known locations are recorded, the gathers may be constructed and analyzed only at those spatial positions, as is done in this study. Nonetheless, even without source-location information, time-shifted gathers may be useful. In that case, they should be flat at a certain point in space and at a certain time. This opens up a window for calibration-free velocity estimation, which is not discussed in this study.

The suggested approach has several limitations. Because average gather properties are measured, using a large number of receivers is important for the stabilization of the objective function calculation and its robustness to noise. In this aspect, using picked traveltimes would be better in terms of inversion convergence. For practical cases, we believe that several dozens of receivers will be required for an effective solution. Given the recent improvements and availability of DAS monitoring, this limitation may soon be alleviated. Another restriction is that input data need to be corrected for source focal mechanism and measurement axis imprint, influencing the phase and amplitude. Otherwise, the coherency values of the gather will spuriously deteriorate. Because we use solely kinematic information, this correction may be conventionally applied and include sign-only compensation. Alternatively, one may use the signal envelope or absolute value at a cost of reduced resolution, but some preprocessing of the data will still be required. For the near-surface field example that we show, more intensive processing is needed, including muting around the first arrivals and removing low-quality or dead traces. A final limitation, most clearly visible when observing the wave-equation synthetic data set, is the potential problem of cycle skipping. It is a common difficulty, shared by most if not all waveform-based inversion methods, most notably full-waveform inversion. Nonetheless, because reasonable initial velocity models may usually be expected in monitoring configurations, cycle skipping will be less severe. It is also possible to coarsely mute recorded data around the first arrivals (P and S) to eliminate trailing events, which might cause cycle skipping. These events, in contrast to reflection seismology, can be considered as noise assuming that the first arrivals are clearly visible.

We want to emphasize that if traveltime picking is conducted correctly, the method may be effectively reduced to operate on picked traveltimes with a different objective function. In this aspect, because our suggested approach uses a ray approximation, there is no fundamental difference between using picks and moveout-corrected gathers. The gathers could also be used to conveniently extract residual traveltime moveout by crosscorrelation. Such traveltime differences, if reliably extracted, can be used to solve a purely kinematic inversion as well. Another advantage of using moveout-corrected gathers, not implemented in this study, is that they may be constructed using a wave-equation formulation. Computational costs would be higher, but propagation would be calculated more precisely, and sharp model contrasts could be accurately handled.

To solve the inverse problem, we opt for a global-optimization approach. We use the CPSO algorithm, but many other choices are possible. Because reasonably good initial structural models and their interpretation are to be expected, adequate model parameterizations for global optimization may be chosen. For example, given a conventional monitoring scenario, approximately 20–30 layers are usually enough for subsurface model representation. Assuming that for each layer velocity, dip, and possibly top are all inverted, we are still inverting for less than 100 parameters — considered a relatively simple problem for global optimization. The convergence rate depends on the number of parameters and the quality of the initial model, but the overall problem dimensionality is within the capabilities of global optimization methods. In addition, the objective function used for inversion is complex and has many local minima. Any local optimization approach will strongly depend on the initial model and will most likely converge to a nonoptimal solution.

We stress that inverted models are not structurally correct. As a single calibration source is used, inverted models can only be expected to explain the scarce input data. In other words, inverted models are, ideally, equivalent to the true model only for the input data because they yield a gather of equivalent flatness measure. As, a consequence, for any source at a different location than the calibration point, the two models are not necessarily equivalent. In our examples, we show that the location results improved after calibration. This is partly because the located sources are relatively close to the calibration one. Parts of the models that are illuminated by the calibration source are roughly those used for event location. It is reasonable to assume that the location quality will thus decrease the farther away sources are from the calibration point. For example, using the perforation shot for velocity calibration and subsequent

Downloaded 04/04/19 to 171.66.208.130. Redistribution subject to SEG license or copyright; see Terms of Use at http://library.seg.org/

location of microseismic events is a promising application because events are expected to be nearby. If the calibration source is, instead, a shot at the surface the suggested methodology would probably fail. Different parts of the model would be illuminated, and velocity updates might be applied to areas of the model that are irrelevant to the location procedure.

Although surface sources would probably be useless for calibration, the method could work well using surface receivers. Because such receivers often suffer from low signal-to-noise ratio, the averaging nature of the objective function could prove useful. Higher resolution is to be expected in the horizontal direction in this case, contrary to the examples shown in this study. Nonetheless, the calibration workflow would be the same up to possible differences in model parameterization. Along with the joint downhole and surface receiver's calibration, it remains open to further research.

Extension of the method to 3D model updates depends only on receiver coverage and computational power. In the field example, because the data coverage is very poor, we show a simple and direct way of adopting a multi-2D approach to 3D model building. However, assuming better coverage and model parameterization, accounting for some lateral variation (e.g., linear gradient, azimuthal dependence, and sectoring), 3D models may be directly inverted. As a further step, anisotropic parameters may also be introduced to the model's parameterization and inverted for.

Although this study shows a conceptual approach, it could benefit from testing on conventional monitoring data. Such tests should include integration with the standard monitoring workflow, including back-propagation, joint P and S analysis, and focal mechanism estimation, to demonstrate the practical usefulness of the suggested method. Thanks to its ability to handle low signal-to-noise-ratio events, incorporating surface monitoring could be effectively used for better model inversion and location stabilization. In addition, assuming a clear separation between different phases, a joint P/S inversion, based on a common source location and origin time, could be easily formulated and implemented as many structural parameters (tops, layer dips . . .) are shared by the P- and S-velocity models.

CONCLUSION

In this study, we advocate the use of time-shifted gathers as a tool for velocity model estimation. These gathers are assumed to be flat only when constructed at the true source location and using the correct velocity model. Their flatness is quantified using the minimum variation criterion, which operates as the objective function in a proposed velocity inversion scheme. The main advantage of using the suggested approach is that it does not require traveltime picking of the data and can be formulated using a wave-equation framework. It can be used on recorded data after radiation pattern and measurement axis effects have been corrected for the phase sign, or on the signal envelope. The method is less prone to noise, maintains original data characteristics, and may be manually used for QC. Because the amount of analyzed data is relatively small and good initial models are to be expected, we utilize a global-optimization approach to the velocity inversion problem. Although model parameterization may be a limiting factor due to computational costs, it is much more resilient to local extremum convergence. In structurally complex synthetic and field-data examples, we show that although inverted velocity models are nonunique and not necessarily close to the true model, they significantly improve the location results. In addition, the location results can be further improved if the origin time of the calibration source is known.

DATA AND MATERIALS AVAILABILITY

Data associated with this research are available and can be obtained by contacting the corresponding author.

REFERENCES

Abelson, M., T. Aksinenko, I. Kurzon, V. Pinsky, G. Baer, R. Nof, and Y. Yechieli, 2018, Nanoseismicity forecasts sinkhole collapse in the Dead Sea coast years in advance: Geology, **46**, 83–86, doi: 10.1130/G39579.

Bardainne, T., and E. Gaucher, 2010, Constrained tomography of realistic velocity models in microseismic monitoring using calibration shots: Geophysical Prospecting, **58**, 739–753, doi: 10.1111/j.1365-2478.2010.00912.x.

Bardainne, T., E. Gaucher, F. Cerda, and D. Drapeau, 2009, Comparison of picking-based and waveform-based location methods of microseismic events: Application to a fracturing job: 79th Annual International Meeting, SEG, Expanded Abstracts, 1547–1551, doi: 10.1190/1.3255144.

Biondi, B., 2006, 3D seismic imaging: SEG.

Brandsberg-Dahl, S., B. Ursin, and M. V. de Hoop, 2003, Seismic velocity analysis in the scattering-angle/azimuth domain: Geophysical Prospecting, **51**, 295–314, doi: 10.1046/j.1365-2478.2003.00370.x.

Cao, W., S. M. Hanafy, G. T. Schuster, G. Zhan, and C. Boonyasiriwat, 2012, High-resolution and super stacking of time-reversal mirrors in locating seismic sources: Geophysical Prospecting, **60**, 1–17, doi: 10.1111/j.1365-2478.2011.00957.x.

Chambers, K., B. D. E. Dando, G. A. Jones, R. Velasco, and S. A. Wilson, 2014, Moment tensor migration imaging: Geophysical Prospecting, **62**, 879–896, doi: 10.1111/1365-2478.12108.

Chambers, K., J. M. Kendall, S. Brandsberg-Dahl, and J. Rueda, 2010, Testing the ability of surface arrays to monitor microseismic activity: Geophysical Prospecting, **58**, 821–830, doi: 10.1111/j.1365-2478.2010.00893.x.

Diller, D. E., and S. P. Gardner, 2011, Comparison of simultaneous downhole and surface microseismic monitoring in the Williston Basin: 81st Annual International Meeting, SEG, Expanded Abstracts, 1504–1508, doi: 10.1190/1.3627487.

Drew, J. E., H. D. Leslie, P. N. Armstrong, and G. Michard, 2005, Automated microseismic event detection and location by continuous spatial mapping: Proceedings of the SPE Annual Technical Conference and Exhibition, Paper 95513, doi: 10.2118/95513-MS.

Earle, P. S., and P. M. Shearer, 1994, Characterization of global seismograms using an automatic-picking algorithm: Bulletin of the Seismological Society of America, **84**, 366–376.

Eisner, L., P. M. Duncan, W. M. Heigl, and W. R. Keller, 2009a, Uncertainties in passive seismic monitoring: The Leading Edge, **28**, 648–655, doi: 10.1190/1.3148403.

Eisner, L., T. Fischer, and J. T. Rutledge, 2009b, Determination of S-wave slowness from a linear array of borehole receivers: Geophysical Journal International, **176**, 31–39, doi: 10.1111/j.1365-246X.2008.03939.x.

Eisner, L., B. J. Hulsey, P. Duncan, D. Jurick, H. Werner, and W. Keller, 2010, Comparison of surface and borehole locations of induced seismicity: Geophysical Prospecting, **58**, 809–820, doi: 10.1111/j.1365-2478.2010.00867.x.

Eisner, L., Y. Zhang, P. Duncan, M. C. Mueller, M. P. Thornton, and D. Gei, 2011, Effective VTI anisotropy for consistent monitoring of microseismic events: The Leading Edge, **30**, 772–776, doi: 10.1190/1.3609092.

Fischer, T., S. Hainzl, L. Eisner, S. A. Shapiro, and J. Le Calvez, 2008, Microseismic signatures of hydraulic fracture growth in sediment formations: Observations and modeling: Journal of Geophysical Research, **113**, 1–12, doi: 10.1029/2007JB005070.

Fuller, B., L. Engelbrecht, R. Van Dok, and M. Sterling, 2007, Diffraction processing of downhole passive monitoring data to image hydrofracture locations: 77th Annual International Meeting, SEG, Expanded Abstracts, 1297–1301, doi: 10.1190/1.2792740.

Gibowicz, S. J., and A. Kjiko, 1994, An introduction to mining seismology: Academic Press.

Grechka, V., A. De La Pena, E. Schisselé-Rebel, E. Auger, and P. Roux, 2015, Relative location of microseismicity: Geophysics, **80**, no. 6, WC1–WC9, doi: 10.1190/geo2014-0617.1.

Grechka, V., P. Singh, and I. Das, 2011, Estimation of effective anisotropy simultaneously with locations of microseismic events: Geophysics, **76**, no. 6, WC143–WC155, doi: 10.1190/geo2010-0409.1.

Haldorsen, J. B., N. Brooks, and M. Milenkovic, 2013, Locating microseismic sources using migration-based deconvolution: Geophysics, **78**, no. 5, KS73–KS84, doi: 10.1190/geo2013-0086.1.

Hogarth, L. J., C. M. Kolb, and J. H. Le Calvez, 2017, Controlled-source velocity calibration for real-time downhole microseismic monitoring: The Leading Edge, **36**, 172–178, doi: 10.1190/tle36020172.1.
Jeremic, A., and P. M. Duncan, 2017, Transmission multicomponent interferometric extended source velocity analysis: 79th Annual International Conference and Exhibition, EAGE, Extended Abstracts, doi: 10.3997/2214-4609.201701226.
Karrenbach, M., D. Kahn, S. Cole, A. Ridge, K. Boone, J. Rich, K. Silver, and D. Langton, 2017, Hydraulic-fracturing-induced strain and microseismic using in situ distributed fiber-optic sensing: The Leading Edge, **36**, 837–844, doi: 10.1190/tle36100837.1.
Lellouch, A., and E. Landa, 2017, Time reversal focusing for velocity estimation: Cross-well acquisition: 87th Annual International Meeting, SEG, Expanded Abstracts, 5620–5624, doi: 10.1190/segam2017-17632416.1.
Lellouch, A., and E. Landa, 2018, Seismic velocity estimation using time-reversal focusing: Geophysics, **83**, no. 4, U43–U50, doi: 10.1190/geo2017-0569.1.
Lellouch, A., and M. Reshef, 2016, Usage of directional common image gathers for shallow seismic source localization: Near Surface Geophysics, **14**, no. 3, 231–241, doi: 10.3997/1873-0604.2016012.
Lellouch, A., and M. Reshef, 2017, Shallow diffraction imaging in an SH-wave crosshole configuration: Geophysics, **82**, no. 1, S9–S18, doi: 10.1190/geo2016-0154.1.
Luu, K., M. Noble, and A. Gesret, 2016, A competitive particle swarm optimization for nonlinear first arrival traveltime tomography: 86th Annual International Meeting, SEG, Expanded Abstracts, 2740–2744, doi: 10.1190/segam2016-13840267.1.
Lyu, B., N. Nakata, and K. J. Marfurt, 2018, A reverse-time migration workflow of passive source with joint imaging conditions: 88th Annual International Meeting, SEG, Expanded Abstracts, 2947–2951, doi: 10.1190/segam2018-2998330.1.
Maxwell, S., 2010, Microseismic: Growth born from success: The Leading Edge, **29**, 338–343, doi: 10.1190/1.3353732.
Maxwell, S., 2014, Microseismic imaging of hydraulic fracturing: Improved engineering of unconventional shale reservoirs: SEG, Distinguished Instructor Series 17.
Maxwell, S. C., J. Rutledge, R. Jones, and M. Fehler, 2010, Petroleum reservoir characterization using downhole microseismic monitoring: Geophysics, **75**, no. 5, 75A129–75A137, doi: 10.1190/1.3477966.
Molyneux, J. B., and D. R. Schmitt, 1999, First-break timing: Arrival onset times by direct correlation: Geophysics, **64**, 1492–1501, doi: 10.1190/1.1444653.
Pei, D., J. A. Quirein, B. E. Cornish, D. Quinn, and N. R. Warpinski, 2009, Velocity calibration for microseismic monitoring: A very fast simulated annealing (VFSA) approach for joint-objective optimization: Geophysics, **74**, no. 6, WCB47–WCB55, doi: 10.1190/1.3238365.
Poli, R., J. Kennedy, and T. Blackwell, 2007, Particle swarm optimization: Swarm Intelligence, **1**, 33–57, doi: 10.1007/s11721-007-0002-0.
Poliannikov, O. V., M. Prange, A. E. Malcolm, and H. Djikpesse, 2014, Joint location of microseismic events in the presence of velocity uncertainty: Geophysics, **79**, no. 6, KS51–KS60, doi: 10.1190/geo2013-0390.1.
Sabbione, J. I., and D. Velis, 2010, Automatic first-breaks picking: New strategies and algorithms: Geophyiscs, **75**, no. 4, V67–V76, doi: 10.1190/1.3463703.
Sen, M. K., and P. L. Stoffa, 2013, Global optimization methods in geophysical inversion: Cambridge University Press.
Senfaute, G., A. Duperret, and J. A. Lawrence, 2009, Micro-seismic precursory cracks prior to rock-fall on coastal chalk cliffs: A case study at Mesnil-Val, Normandie, NW France: Natural Hazards and Earth System Sciences, **9**, 1625–1641, doi: 10.5194/nhess-9-1625-2009.
Shuck, T., D. E. Diller, B. Fish, P. Smith, and K. Wallace, 2015, Surface microseismic in an extreme environment: The Leading Edge, **34**, 936–943, doi: 10.1190/tle34080936.1.
Šílený, J., and A. Milev, 2008, Source mechanism of mining induced seismic events: Resolution of double couple and non double couple models: Tectonophysics, **456**, 3–15, doi: 10.1016/j.tecto.2006.09.021.
Symes, W. W., 2008, Migration velocity analysis and waveform inversion: Geophysical Prospecting, **56**, 765–790, doi: 10.1111/j.1365-2478.2008.00698.x.
Tonnellier, A., A. Helmstetter, J. P. Malet, J. Schmittbuhl, A. Corsini, and M. Joswig, 2013, Seismic monitoring of soft-rock landslides: The super-sauze and valoria case studies: Geophysical Journal International, **193**, 1515–1536, doi: 10.1093/gji/ggt039.
Tucker, R. E., J. R. Mckenna, M. H. Mckenna, and M. S. Mattice, 2007, Detecting underground penetration attempts at secure facilities: Engineer, **1**, 31–34.
Urbancic, T. I., and J. Rutledge, 2000, Using microseismicity to map cotton valley hydraulic fractures: 70th Annual International Meeting, SEG, Expanded Abstracts, 1444–1448, doi: 10.1190/1.1815676.
Wang, H., and T. Alkhalifah, 2018, Microseismic imaging using a source function independent full waveform inversion method: Geophysical Journal International, **214**, 46–57, doi: 10.1093/gji/ggy121.
Witten, B., and J. Shragge, 2017, Image-domain velocity inversion and event location for microseismic monitoring: Geophysics, **82**, no. 5, KS71–KS83, doi: 10.1190/geo2016-0561.1.
Wuestefeld, A., O. Al-Harrasi, J. P. Verdon, J. Wookey, and J. M. Kendall, 2010, A strategy for automated analysis of passive microseismic data to image seismic anisotropy and fracture characteristics: Geophysical Prospecting, **58**, 755–773, doi: 10.1111/j.1365-2478.2010.00891.x.
Zhebel, O., and L. Eisner, 2015, Simultaneous microseismic event localization and source mechanism determination: Geophysics, **80**, no. 1, KS1–KS9, doi: 10.1190/geo2014-0055.1.

Downloaded 04/04/19 to 171.66.208.130. Redistribution subject to SEG license or copyright; see Terms of Use at http://library.seg.org/